Vertical changes in volatile organic compounds (VOCs) and impacts on photochemical ozone formation

Xiao-Bing Li[1], Bin Yuan[1,*], Yibo Huangfu[1], Suxia Yang[2], Xin Song[1], Jipeng Qi[1], Xianjun He[1], Sihang Wang[1], Yubin Chen[1], Qing Yang[1], Yongxin Song[1], Yuwen Peng[1], Guiqian Tang[3, 4], Jian Gao[5], Dasa Gu[6], Min Shao[1]

[1] College of Environment and Climate, Institute for Environmental and Climate Research, Guangdong-Hongkong-Macau Joint Laboratory of Collaborative Innovation for Environmental Quality, Jinan University, Guangzhou 511443, China

[2] Guangzhou Research Institute of Environment Protection Co., Ltd., Guangzhou 510620, China

[3] State Key Laboratory of Atmospheric Environment and Extreme Meteorology, Institute of Atmospheric Physics, Chinese Academy of Sciences, Beijing 100029, China

[4] University of Chinese Academy of Sciences, Beijing, 100049, China

[5] State Key Laboratory of Environmental Criteria and Risk Assessment, Chinese Research Academy of Environmental Sciences, Beijing 100012, China

[6] Guangdong−Hongkong−Macau Joint Laboratory of Collaborative Innovation for Environmental Quality and Division of Environment and Sustainability, The Hong Kong University of Science and Technology, Hong Kong 999077, China

[*] Corresponding author: Bin Yuan (byuan@jnu.edu.cn)

Abstract

Volatile organic compounds (VOCs) play crucial roles in regulating the formation of tropospheric ozone. However, limited knowledge on the interactions between vertical VOC variations and photochemical ozone formation in the planetary boundary layer (PBL) has hindered effective ozone control strategies, especially in large cities. In this study, we investigated the vertical changes in concentrations, compositions, and key driving factors of a large suite of VOCs using online gradient measurements taken from a 325 m tall tower in urban Beijing. The impact of these vertical VOC variations on photochemical ozone formation were also analyzed using box model simulations. Our results indicate that VOCs exhibited distinct vertical variation patterns due to their differences in sources and chemical reactivities, along with the diurnal evolution of the PBL. During daytime, reactive VOCs (e.g., hydrocarbons) are rapidly oxidized as they mix upwards, accompanied by the formation and accumulation of oxygenated VOCs (OVOCs) in the middle and upper layers. In addition, the photochemical formation of ozone responds positively to changes in both NOx and VOCs. As a result, the production rate of ozone declines with height due to the simultaneous decreases in concentrations of reactive VOCs and NOx, but remains high in the middle and upper layers. The strong production of ozone aloft is primarily driven by the presence of high OVOCs concentrations. Therefore, careful consideration should be given to the vertical variations in both photochemical ozone production rates and formation regimes in the whole PBL when developing regional ozone control strategies.

1 Introduction

Volatile organic compounds (VOCs) are crucial constituents of atmospheric chemicals *(Li et al., 2022c)* and play important roles in regulating the atmospheric oxidation capacity and contributing to the photochemical formation of tropospheric ozone *(Zhao et al., 2022; Yang et al., 2024b)*. Ozone is a major air pollutant in urban environments, with increasing trends reported globally over recent decades *(Fleming et al., 2018; Cooper et al., 2020)*, despite stringent measures to control its precursor emissions *(Wang et al., 2020b; Yeo and Kim, 2021; Li et al., 2022b; Perdigones et al., 2022)*. As highlighted in previous studies, reducing emissions of reactive VOCs is key to controlling ozone pollution at present and in the foreseeable future *(Zhao et al., 2022; Wang et al., 2024)*.

The primary prerequisite for effective regional ozone pollution control is the determination of the photochemical ozone formation regime *(Souri et al., 2020; Zhao et al., 2022)*, which facilitates the development of reduction schemes for key precursor emissions *(Ou et al., 2016; Wang et al., 2019)*. The main challenges in controlling ozone pollution stem from the complex compositions of its precursors (e.g., VOCs and NOx) in ambient air *(Guo et al., 2017; Wu et al., 2020; Li et al., 2022c)*, as well as the complicated responses of photochemical ozone formation to changes in these precursors *(Shao et al., 2021; Perdigones et al., 2022)*. Furthermore, the interactions between vertical variations of ozone precursors and ozone formation remain unclear *(Tang et al., 2017; Sun et al., 2018; Li et al., 2024)*, adding to the complexity of ozone pollution control.

In most cases, the identification of key ozone precursors has been conducted using ground-level observations *(Qi et al., 2021; Lu et al., 2022)* or compiled source emission inventories *(Ou et al., 2015; An et al., 2021; Wang et al., 2022b)*. While these methods are undoubtedly helpful in determining key ozone precursors and corresponding reduction strategies, they often encounter unexpected uncertainties in urban regions. *(Mo et al., 2018; Mo et al., 2020)*. Consequently, ground-level measurements of ozone

69 precursors have been favored to constrain model calculations *(Lu et al., 2012; Wang et*

70 *al., 2022a; Yang et al., 2022)* or provide empirical evidence for hypothesized theories

71 *(Hofzumahaus et al., 2009; Wang et al., 2022c)*. However, these ground-level

72 measurements cannot fully characterize atmospheric chemical processes in the entire

73 planetary boundary layer (PBL) due to strong vertical variations in precursor

74 concentrations *(Velasco et al., 2008; Li et al., 2018; Sun et al., 2018)*.

75   Ambient VOCs, as crucial ozone precursors, are composed of myriad species *(Wu*

76 *et al., 2020; Gkatzelis et al., 2021; Ye et al., 2021; He et al., 2022)* and serve diverse

77 functions in photochemical ozone formation *(Vo et al., 2018; Li et al., 2022a; Zhang et*

78 *al., 2022)*. Owing to the impact of variations in emission sources, chemical removal,

79 advection and convection transport, and secondary formation, the concentration and

80 composition of VOCs typically display notable vertical variability within the PBL,

81 especially in urban areas *(Li et al., 2022c)*. The ozone formation regime likely

82 undergoes significant transitions from the ground to the upper boundary layer *(Li et al.,*

83 *2024; Liu et al., 2024a)*. Ozone generated throughout the PBL can influence surface

84 ozone levels due to enhanced atmospheric vertical mixing during the day. Consequently,

85 it is imperative to comprehend the vertical variations and principal determinants of

86 VOCs, as well as their effects on photochemical ozone formation within the PBL.

87   With the rapid development of cities in the recent two decades in China, a large

88 number of pollution-emitting industries and factories have been relocated from city

89 centers to alleviate air pollution. Concurrently, there's been a swift increase in the

90 ownership of electric vehicles *(Guo et al., 2021)*. These shifts in energy consumption

91 have driven the change in concentrations and compositions of VOCs in major cities like

92 Beijing *(Liu et al., 2024b)*, subsequently affecting photochemical ozone formation

93 *(Wang et al., 2024)*. However, the vertical variations and key drivers of VOCs and their

94 impacts on photochemical ozone formation in the urban PBL remain elusive. A primary

95 hurdle in studying these vertical changes in photochemical ozone formation is the

96 scarcity of reliable vertical VOC data *(Dieu Hien et al., 2019; Li et al., 2022c)*.

97 Engaging in vertical profiling of VOCs, ensuring all necessary species represented and

98 obtaining sufficient sample size, is especially challenging in the lower PBL where

99 atmospheric chemical reactions are most intense *(Benish et al., 2020; Kim et al., 2021)*.

100 Previous studies on vertical distributions of photochemical ozone formation in the

101 PBL have been conducted using measurements of a limited number of VOC species

102 and samples *(Zhang et al., 2018; Benish et al., 2020; Geng et al., 2020)*. In this study,

103 online gradient measurements of ozone, NOx, and a large suit of VOCs were made on

104 a 325 m tall tower in urban Beijing during the summer of 2021. Additionally, box model

105 simulations constrained by the gradient measurements were performed to analyze the

106 vertical variations and key drivers of VOCs as well as their impacts on photochemical

107 ozone formation.

2 Methods and materials

2.1 Description of the site, instrument, and field campaign

110 The data utilized in this study was derived from an intensive field campaign

111 conducted at the Beijing Meteorological Tower (BMT: 39°58′ N, 116°23′ E) between

112 July 6 and August 4, 2021. The BMT has a height of 325 m and is located in the northern

113 part of downtown Beijing, positioned between the third and fourth ring roads (Fig. S1).

114 A vertical observation system, established using long perfluoroalkoxy alkane (PFA)

115 Teflon tubes (OD: 1/2 in.), was used to make online gradient measurements of ozone,

116 NOx, and a set of VOCs on the BMT. Five specific heights, namely 15, 47, 102, 200,

117 and 320 m above ground level, were selected to mount the tube inlets, as depicted in

118 Fig. S3. An additional inlet, situated approximately 5 m above ground level, was

119 mounted on the rooftop of the observation room that was adjacent to the tower.

120 Consequently, the vertical observation system totally included a total of six sampling

121 inlets. The sampling inlet at the 15 m height was not utilized during this field campaign.

122 Filters were installed downstream of the tubing inlets on the tower to remove fine

123 particles. A rotary vane vacuum pump was used to simultaneously and continuously

124 draw sample air from the five tubes, ensuring that all tubes were flushed by ambient air

125   to reduce tubing delays of sticky organic compounds *(Pagonis et al., 2017; Liu et al.,*

126   *2019)*. Five critical orifices were employed to control the flow rate of the air stream in

127   each tubing, resulting in flow rates ranging between 15 and 20 standard liter per minute

128   (SLPM). Instruments drew sample air from the five tubes sequentially through a Teflon

129   solenoid valve group at designated time intervals. The switching time intervals of the

130   Teflon solenoid valve group were set as 4 minutes during this field campaign. The

131   measurements of trace gases in the first and last 1 minute of a four-minute period were

132   discarded to eliminate cross interferences between different inlet heights. Detailed

133   information on the vertical observation system and the assessment of trace gas

134   measurements through hundreds of meters long PFA tubes has been provided in our

135   previous works *(Li et al., 2023; Song et al., 2024; Yang et al., 2024a)*.

136   Ozone was measured using the ultraviolet photometry method (49i, Thermo Fisher

137   Scientific Inc., USA). NO, NO_2, and NOx were measured using the chemiluminescence

138   method (42i, Thermo Fisher Scientific Inc., USA). Gradient measurements of ozone

139   and NOx were conducted at a time resolution of 10 seconds. The photolysis frequencies

140   of NO_2, represented by $j(NO_2)$, were measured by a spectrometer (PFS-100, Focused

141   Photonics Inc., China) situated on the rooftop of the observation room and have a time

142   resolution of 8 seconds. In situ measurements of meteorological parameters including

143   wind speed, air temperature, and relative humidity were made at 15 heights between 8

144   m and 320 m on the BMT with a time resolution of 20 seconds. Planetary boundary

145   layer   height   (PBLH)   was   obtained   from   the   Air   Resources   Laboratory

146   (*https://ready.arl.noaa.gov/READYamet.php, last access: 10 June 2024*) and was

147   linearly interpolated to hourly values based on the initial time resolutions of three hours

148   *(Li and Fan, 2022)*.

149   A high-resolution proton-transfer-reaction quadrupole interface time-of-flight

150   mass spectrometer (PTR-ToF-MS, Ionicon Analytik, Austria) was employed to measure

151   VOCs at a time resolution of 10 seconds. The PTR-ToF-MS used both hydronium ion

152   (H_3O^+) *(Yuan et al., 2017; Wu et al., 2020; Li et al., 2022c)* and nitric oxide ion (NO^+)

153   *(Wang et al., 2020a)* as reagent ions. These two reagent ions were automatically

154   switched every 60 min for H_3O^+ and every 22 min for NO^+ throughout the campaign.

155   The PTR-ToF-MS operated at an E/N value of approximately 120 Td in H_3O^+ mode

156   and an E/N value of around 60 Td in NO^+ mode. Instrument backgrounds were

157   automatically measured during the last two minutes of each operation mode by passing

158   ambient air through a platinum catalyst heated to 365 ℃. A gas standard containing 39

159   VOC species was used to calibrate the PTR-ToF-MS daily. Sensitivities for the

160   remaining species were determined based on reaction kinetics of the PTR-ToF-MS *(Wu*

161   *et al., 2020)*. Impacts of ambient humidity on the PTR-ToF-MS measurements were

162   corrected by using humidity-dependence curves of VOCs obtained in our laboratory

163   *(Wang et al., 2020a; Wu et al., 2020)*. Carbon dioxide (CO_2 in dry air) and humidity

164   were measured using a CO_2 and H_2O gas analyzer (Li-840A, Licor Inc., USA) at a time

165   resolution of 10 seconds.

166   Gradient measurements of the total OH reactivity (OHR) of atmospheric trace

167   gases were made using the improved comparative reactivity method (ICRM) developed

168   by our team *(Wang et al., 2021a)* from July 28 to 31. In addition, gradient measurements

169   of carbon monoxide (CO), methane (CH_4), CO_2, and H_2O were simultaneously

170   measured using the cavity ring-down spectroscopy (CRDS) method (G-2401, Picarro

171   Inc., USA) at a time resolution of 10 seconds from May 15 to June 25. Sulfur dioxide

172   (SO_2) was measured using the ultraviolet fluorescence method (43i, Thermo Fisher

173   Scientific Inc., USA) at a time resolution of 10 seconds from June 25 to August 3. The

174   total OHR of VOCs, denoted by OHR_{VOCs}, can be estimated by excluding those of the

175   inorganic species (namely ozone, NOx, CO, SO_2, and CH_4). It should be noted that

176   gradient measurements of CH_4 and CO were not made during July 28-31, and their

177   average concentrations in daytime (11:00-16:00 LT) between May 15 and June 25 at 5

178   m were used for all altitudes to calculate OHR_{VOCs}. This method will bring minor

179   uncertainties due to the minor vertical differences in concentrations of CH_4 and CO in

180   daytime (Fig. S4). The OHR of VOCs can also be calculated by summing the products

181   of their measured concentrations and their reaction rate coefficients with OH radicals,

182   as formulated in Eq. (1):

$$\text{OHR} = \sum k^i_{OH-R}[VOC_i] \qquad \text{Eq. (1)}$$

where k^i_{OH-R} is the reaction rate coefficient of the ith VOC species with OH radical and $[VOC_i]$ is the concentration of the ith VOC species.

2.2 Estimation of NMHC concentrations at the BMT site

The PTR-ToF-MS is limited in its ability to measure VOC species with proton affinities higher than H_2O (691 kJ mol^{-1}) when operating in the H_3O^+ mode *(Yuan et al., 2017)*. This limitation results in the absence of certain nonmethane hydrocarbons (NMHCs), such as alkanes and many alkene species, which play important roles in photochemical ozone formation. To obtain a comprehensive understanding of vertical variations in concentrations, compositions, and environmental impacts of VOCs, this study estimated the vertical profiles of those unmeasured NMHC species based on the concentrations of measured VOCs using the PTR-ToF-MS. Detailed information on estimation of NMHC concentrations is provided in SI.

2.3 Box model setup

A zero-dimension box model (F0AM) coupled with the Master Chemical Mechanism (v3.3.1) *(Wolfe et al., 2016; Yang et al., 2022)* was used to compute the production rate of ozone, denoted by P(O$_3$) as formulated in Eq. (2):

$$\text{P}(O_3) = k_{HO_2+NO}[HO_2][NO] + \sum k^i_{RO_2+NO}[R^iO_2][NO] \qquad \text{Eq. (2)}$$

$$k_{RO_2+NO}[RO_2][NO]$$

where [HO$_2$] and [NO] is the concentrations of HO$_2$ and NO, [R^{i}O$_2$] is the concentration of the ith organic peroxyl radical. The relative incremental reactivity (RIR) of photochemical ozone production to changes in different precursors was determined using Eq. (3):

$$\text{RIR}(X) = \frac{\left[P^S_{O_x}(X) - P^S_{O_x}(X - \Delta X)\right]/P^S_{O_x}(X)}{\Delta S(X)/S(X)} \qquad \text{Eq. (3)}$$

204 where X represents ozone precursors, $P_{O_x}^S(X)$ is the contribution of X to the production

205 rate of Ox, ΔX is the amount of change in ozone precursors, $S(X)$ is the initial

206 concentration of X. RIR values were used to discern sensitivities of photochemical

207 ozone formation to changes in precursor gases. A positive RIR(X) value suggests that

208 an increase in X enhances ozone formation, while a negative RIR value indicates that

209 an increase in X inhibits ozone formation.

210   Model calculations were constrained by measurements of ozone, NOx, CO, a suit

211 of VOCs, air temperature, and relative humidity. In addition to the measured or

212 estimated concentrations of NMHCs, nine oxygenated VOC (OVOC) species (Table

213 S1) measured by PTR-ToF-MS were used to constrain the model calculation. The

214 model was run in a time-dependent mode with a time resolution of 5 minutes and a

215 spin-up period of 2 days *(Lu et al., 2012; Wang et al., 2022c)*. The dry deposition

216 velocity of ozone was set as 0.27 cm s^{-1} when calculating P(O$_3$) 5 m and was zeroed

217 out when calculating P(O$_3$) at other heights.

3   Results and discussions

3.1   Temporal and vertical variations in concentrations of trace gases

220   As shown in Fig. 1, the meteorology in Beijing was characterized by high air

221 temperature (27.3±2.9 °C), high humidity (83.9%±16.2%), and gentle winds (1.1±0.4

222 m s^{-1}) throughout the campaign. The intense solar radiation, elevated air temperature,

223 and mild winds favored the photochemical formation and accumulation of ozone,

224 leading to frequent occurrences of ozone pollution episodes. Fig. 1 also presents time

225 series of mixing ratios of ozone and its selected precursors (namely isoprene, toluene,

226 monoterpenes, and NOx) along with j(NO$_2$) measured at 5 m. The campaign mean

227 ozone mixing ratio was 45.6±25.3 ppb, but the maximum hourly mean ozone mixing

228 ratio reached 129.3 ppb, indicating strong photochemical reactions in urban Beijing

229 during the campaign. Surface ozone concentrations exhibited a typical diurnal variation

230 pattern with the maximum occurring at 16:00 LT (Fig. S6), implying its predominant

231 source from local photochemical production.

232 Isoprene is a typical tracer of biogenic emissions and is also a highly reactive VOC

233 species *(Atkinson and Arey, 2003)*. Isoprene had a campaign mean mixing ratio of

234 0.7±0.6 ppb. The average diurnal profile of isoprene at 5 m has a unimodal pattern with

235 the maximum occurring at 14:00 LT (Fig. S6), exhibiting strong dependence on solar

236 radiation. Monoterpenes were also generally recognized as typical tracers of biogenic

237 emissions *(Gómez et al., 2020)* and have a campaign mean mixing ratio of 0.3±0.3 ppb.

238 The average diurnal profile of monoterpenes was characterized by low mixing ratios in

239 daytime with two peaks occurring at 05:00 and 20:00 LT, respectively.

240 Toluene and NOx are recognized as typical tracers of anthropogenic emissions in

241 urban regions *(Niu et al., 2017; Li et al., 2022c)*, with campaign mean mixing ratios of

242 0.7±0.7 and 8.1±4.8 ppb, respectively. The average diurnal profiles of toluene and NOx

243 at 5 m exhibited similar variations with larger values at night than during the day. Based

244 on the measured concentrations and diurnal variations of ozone and its key precursors

245 at ground level, it can be inferred that urban Beijing is experiencing severe ozone

246 pollution, which is predominantly contributed by local photochemical production. As

247 key ozone precursors, ambient concentrations of VOCs are contributed by the mixture

248 of anthropogenic and biogenic sources.

249 Fig. 2 shows the average diurnal and vertical variations in mixing ratios of ozone,

250 NOx, Ox (O_3+NO_2), and six selected VOC species (three hydrocarbons and three

251 OVOCs) within the measurement height range of 5-320 m. High mixing ratios of ozone

252 were observed in the afternoon following the enhancement of solar radiation, which

253 was consistent with the diurnal change pattern of ozone concentrations at the ground

254 level. The vertical gradients of ozone mixing ratios were positive throughout the day

255 but substantially enhanced at night (Fig. 3). The lower ozone mixing ratios near the

256 surface than aloft were mainly caused by the enhancement of dry deposition and NO

257 titration *(Brown et al., 2007; Ma et al., 2013; Li et al., 2022b)*.

258   NOx is a primary pollutant and mainly contributed by vehicular exhausts in urban

259   regions. In contrast to ozone, NOx mixing ratios were low in daytime and exhibited

260   negative vertical gradients throughout the day, as shown in Figs. 2B and 3A-B. In

261   nighttime, large amounts of local NOx emissions were trapped and accumulated in a

262   shallow boundary layer (<100 m). NOx concentrations rapidly decreased with height

263   even in the overlying residual layer due to the suppression of turbulence vertical mixing.

264   With the onset of sunlight, the PBL rapidly expanded due to the surface heating effect.

265   The accumulated high concentrations of NOx in the shallow nocturnal boundary layer

266   were thereupon diluted and removed by photochemical reactions.

267   Ox is frequently used as a conserved metric to investigate temporal and spatial

268   variability of ozone by eliminating the NO titration effect. As shown in Fig. 2C, the

269   mixing ratios of Ox had similar diurnal and vertical variation patterns to those of ozone,

270   but the vertical gradients of Ox were weaker than those of ozone. This result suggests

271   that the vertical distribution of NO concentrations played an important role in regulating

272   the vertical change of ozone concentrations. The enhanced positive gradients of ozone

273   mixing ratios at night were predominantly due to the strict suppression of turbulence

274   vertical mixing *(Geyer and Stutz, 2004)*. The higher concentrations of ozone aloft are

275   considered as the residual of the ozone produced in the daytime PBL and have been

276   recognized as an important reservoir for the enhancement of surface ozone in morning

277   periods *(Kaser et al., 2017; Li and Fan, 2022; He et al., 2023)*.

278   Benzene and toluene demonstrated similar diurnal and vertical variations to NOx,

279   with low concentrations in daytime and high concentrations at night, as shown in Figs.

280   2D-F and 3A-B. The concentrations of both benzene and toluene decreased with height

281   throughout the day, confirming their primary emissions from ground-level sources.

282   However, unlike benzene, the diurnal and vertical variations of toluene were more

283   pronounced. Isoprene emissions are highly dependent on solar radiation, resulting in its

284   higher concentrations in the early afternoon compared to other times of the day.

285   Isoprene mixing ratios also exhibited strong negative vertical gradients below 320 m

286   throughout the day. In contrast to toluene, isoprene concentrations decreased more

287 rapidly with height in the daytime. For instance, the mixing ratios of isoprene decreased

288 by approximately 70% from 5 to 320 m in the daytime, while it was only 30% for

289 toluene.

290   Fig. 3A-B show the average vertical profiles of the NMHCs, normalized to their

291 respective ground-level concentrations measured by the PTR-ToF-MS in daytime and

292 nighttime. The normalized mixing ratios of the NMHCs exhibited significantly

293 differentiated gradients in daytime. In contrast, apart from monoterpenes, the

294 differences in vertical gradients of the normalized vertical profiles for other NMHCs

295 were relatively small at night. The differentiated vertical gradients of the NMHCs in

296 daytime were primarily caused by their intrinsic chemical reactivities, such as reactions

297 with OH radicals. As shown in Fig. 4, concentration ratios of the NMHC species

298 between 320 m and 5 m with k_{OH} values lower than 2.5×10^{-11} cm^{-3} molecule^{-1} s^{-1}

299 exhibited slight variability and rapidly declined with the further increases in k_{OH}. The

300 lower NMHC concentrations at higher altitudes were predominantly caused by the

301 combined effects of atmospheric diffusion and chemical removal *(Sangiorgi et al.,*

302 *2011)*.

303   Considering the effects of atmospheric diffusion and chemical removal by

304 reactions with OH radicals, concentration ratios of NMHC species between 320 m and

305 5 m in daytime can be estimated using Eq. (4):

$$y = A \times \exp(-k_{OH}[OH]\Delta t) \qquad \text{Eq. (4)}$$

306 where *y* represents concentration ratios of the NMHC species between two altitudes, A

307 represents the effect of atmospheric dilution, k_{OH} is the reaction rate coefficient of

308 NMHCs with OH radicals, [OH] is the concentration of OH radical, Δt is the

309 turbulence mixing time scale between the two altitudes. The term $[OH]\Delta t$ thus refers

310 to the exposure of NHMCs to OH radicals between the two altitudes. As shown in Fig.

311 4, the average concentration ratios of NMHCs between 320 m and 5 m in daytime

312 during the campaign can be well reproduced using Eq. (4) with the coefficients A of

313 0.88 and $[OH]\Delta t$ of 1.0×10^{10} molecules cm^{-3} s. Atmospheric diffusion processes have

314 same impact on the vertical distributions of all trace gases. The differences in vertical

315 gradients of NMHCs were mainly determined by the differences in their chemical
316 removal rates without considering influences from advection transport.

317   Methanol, as one of the most abundant OVOC species in the atmosphere, had its
318 lowest concentrations during daytime and displayed negative vertical gradients
319 throughout the day, as shown in Fig. 2G. The vertical and diurnal variations of methanol
320 suggest that its ambient concentrations in urban Beijing were mainly contributed by
321 local primary emissions. Conversely, formaldehyde and MVK+MACR (the first-
322 generation oxidation products of isoprene), as the photochemical oxidation products of
323 NMHCs, had higher concentrations during daytime than at night and exhibited
324 relatively weak vertical concentration gradients (Fig. 2H-I). This is mainly because
325 these OVOCs are produced from the oxidation of NMHCs during turbulence vertical
326 mixing and will accumulate in high altitudes. These phenomena were also observed for
327 other OVOC species, as shown in Fig. 3.

328   The vertical and diurnal variations in concentrations of ozone, NOx, and VOCs
329 are intricately governed by their sources, chemical reactivities, and the evolution of the
330 PBL (namely the vertical dilution conditions). A significant accumulation of VOCs in
331 the shallow nocturnal PBL is subsequently vertically diluted and chemically removed
332 during daytime, thereby impacting the photochemical formation of ozone within the
333 daytime PBL. In addition, the observed vertical changes in concentrations of VOCs
334 imply that they will play distinct roles in contributing to photochemical ozone
335 formation.

336 3.2 Vertical variations in contributions of VOCs to OHR

337   During the daytime, VOCs are primarily oxidized by OH radicals and contribute
338 to the photochemical formation of ozone. To provide an overview on the vertical
339 variations in contributions of different VOCs to OHR, another 1204 ions measured by
340 the PTR-ToF-MS and can be quantified were used for analysis. All the VOCs were
341 classified into three large categories, namely C_xH_y (including alkanes, alkenes,
342 aromatics, and other hydrocarbons; 121 species), OVOCs ($C_xH_yO_1$, 121 species;

343     $C_xH_yO_2$, 120 species; $C_xH_yO_{\geq 3}$, 256 species), and N/S-containing (653 species), as

344   shown in Fig.5. Acetylene is included in alkenes.

345   Fig. 5A illustrates that the total mixing ratios of VOCs in daytime exhibited a slight

346   downward trend from 5 m to 320 m, primarily due to the rapid decrease in mixing ratios

347   of the C_xH_y category. The total mixing ratios of the C_xH_y category decreased from 16.8

348   to 10.6 ppb from 5 m to 320 m, with alkanes making the largest contribution, followed

349   by alkenes, aromatics, and other C_xH_y. Alkanes constituted 58% of the total mixing

350   ratios of C_xH_y at 5 m, but this proportion increased to 65% at 320 m. The fractional

351   contributions of alkenes and aromatics in the total mixing ratios of C_xH_y slightly

352   declined from 28% to 22% and from 12% to 10%, respectively, between these two

353   altitudes. As for OVOCs, the $C_xH_yO_1$ category was the most abundant among the

354   measurements, contributing to 52%-58% of the total mixing ratios at the five heights,

355   followed by the $C_xH_yO_2$ (8%-10%), and $C_xH_yO_{\geq 3}$ (2%) categories. The mixing ratios of

356   the N/S-containing category slightly varied around 2.8 ppb between 5-320 m,

357   contributed to approximately 6% of the total VOC concentrations.

358   Similar to the vertical variations in concentrations, OHRs of the C_xH_y category,

359   denoted by OHR_{CH}, also rapidly decreased from 6.9 s^{-1} to 2.5 s^{-1} between 5 and 320 m,

360   accounting for 52%-31% in the total OHRs of VOCs (Fig. 5B). Fractional contributions

361   of alkenes (40-18%), alkanes (5%), and aromatics (5%-4%) to the total OHRs of VOCs

362   all exhibited decreasing tendencies from 5 m to 320 m. The total OHRs of alkenes

363   decreased more quickly from 5 to 320 m than those of alkanes and aromatics. OHRs of

364   the other C_xH_y category stabilized at approximately 0.3 s^{-1} below 320 m, exhibiting an

365   increasing contribution (2%-4%) to the total OHRs of VOCs with the increase in height.

366   The OHRs of other VOC categories only slightly varied without exhibiting a clear

367   variation trend from 5 to 320 m during the day. As a result, fractional contributions of

368   the $C_xH_yO_1$ (27%-42%), $C_xH_yO_2$ (12%-18%), and $C_xH_yO_{\geq 3}$ (5%-7%), and N/S-

369   containing (2%-4%) categories in the total OHRs of VOCs all increased with height.

370   The increased contributions of OVOCs and N/S-containing species to the total

371 concentrations and OHRs of VOCs implied that air masses became more aged with the
372 increase in height.

373 As depicted in Fig. 6A-B, high OHR_{CH} values were mainly constrained in the PBL
374 and is mainly contributed by biogenic hydrocarbons, specifically isoprene, during
375 daytime due to their high OH reactivities and enhanced emissions. The fractional
376 contributions of isoprene in OHR_{CH} decreased rapidly with increasing height (Fig. 7A).
377 For instance, isoprene accounted for a campaign median fraction of 58% in OHR_{CH} at
378 5 m in daytime, making it a frequent contributor to photochemical ozone formation in
379 urban regions. However, this faction decreased to 38% at 320 m. Therefore, it can be
380 speculated that the total contributions of hydrocarbons to the total OHRs of VOCs will
381 also rapidly decline from 320 m to the top of the PBL, which typically ranges between
382 several hundreds of meters to approximately 2~3 km in daytime (Fig. S7).

383 The total concentrations and OHRs of OVOCs only slightly decreased with the
384 increase in height below 320 m in daytime, as shown in Fig. 6C-D. This is consistent
385 with the results of *(Wang et al., 2021b)*, which observed high concentrations of OVOCs
386 in the upper PBL. Consequently, the ratio of OHR_{OVOC} to OHR_{CH}, denoted by
387 OHR_{OVOC}/OHR_{CH}, rapidly increased from 0.87 at 5 m to 2.6 at 320 m (Fig. 7A). This
388 suggests that OVOCs may play more important roles in regulating the photochemical
389 ozone formation in the middle and upper layers. To assess their potential roles in
390 contributing to the photochemical ozone formation throughout the PBL, we calculated
391 the mean OHRs (MOHR) of different VOC categories in daytime using Eq. (5):

$$MOHR(X) = (\sum ([X]_i + [X]_{i-1})(h_i - h_{i-1})/2)/(320 - 5) \qquad \text{Eq. (5)}$$

392 where $MOHR(X)$ is the MOHR of the VOC category X, $[X]_i$ is the concentration of
393 X at the ith altitude (namely 5, 47, 102, 200, and 320 m for h_i) above ground level.

394 As shown in Fig. 7B, the campaign median MOHR for isoprene was 1.7 s^{-1} and
395 accounted for 48% of the campaign median MOHR of the C_xH_y category. This fraction
396 was significantly lower than that of isoprene (57%) in OHR_{CH} at 5 m. In addition, the
397 campaign median MOHR of the C_xH_y category (3.5 s^{-1}) was also significantly lower

than the OHR_{CH} (6.0 s^{-1}) at 5 m. By contrast, the campaign median MOHR of OVOCs (4.8 s^{-1}) was comparable to that of OHR_{OVOC} (4.9 s^{-1}) at 5 m. As unsaturated hydrocarbons, most alkene species are more reactive than alkanes and aromatics *(Atkinson and Arey, 2003)*. As a result, alkenes had dominant contributions to the MOHR of the C_xH_y category and the OHR_{CH} at 5 m in daytime. As shown in Fig. 7C, the campaign mean OHRs of alkanes, alkenes, and aromatics at 5 m in daytime were 0.7, 5.2, and 0.7 s^{-1}, respectively, accounting for 10%, 75%, and 10% of the OHR_{CH}. However, the campaign mean MOHRs of alkanes, alkenes, and aromatics were 0.5, 2.7, and 0.5 s^{-1}, respectively, accounting for 12%, 68%, and 12% of the MOHR of NMHC. We can also expect that the total contributions of alkenes to the MOHR of the C_xH_y category in daytime will significantly decrease if their vertical distributions in the whole PBL are considered.

This study investigated and compared the vertical profiles of measured OHR_{VOCs} and calculated OHR_{CH} during daytime over the period of July 28-31, as shown in Fig. 7D. The campaign median of the measured OHR_{VOCs} exhibited a slow decrease from 38.4 s^{-1} at 5 m to 25.4 s^{-1} at 320 m. As anticipated, the OHR_{CH}/OHR_{VOCs} ratio declined rapidly from 16% to 7% from 5 to 320 m. It is important to note that the small OHR_{CH}/OHR_{VOCs} ratio and its declining trend with the increasing height do not imply the insignificant roles of hydrocarbons in regulating the secondary pollutant formation in higher altitudes. The measured concentrations of hydrocarbons are merely the remnants of chemical reactions. The oxidation products of NMHCs, such as OVOCs and organic nitrates, formed during vertical mixing in daytime, will continue to participate in atmospheric chemical reactions.

3.3 Vertical variations in photochemical ozone formation

The surface ozone budget is intimately linked to the vertical variations of photochemical ozone formation throughout the PBL. Previous studies have consistently reported that the photochemical formation of ozone, encompassing both P(O$_3$) and ozone formation regimes (namely the NOx-limited, VOCs-limited, and transition

426 regimes), are highly dependent on the change in its precursors *(Shao et al., 2021; Yang*

427 *et al., 2022)*. Consequently, any changes in the concentrations and compositions of

428 VOCs and NOx within the PBL will inevitably lead to alternations in the vertical

429 distribution of $P(O_3)$ and ozone formation regimes *(Tang et al., 2017; Li et al., 2024)*.

430   Fig. 8A illustrates the average dependence of $P(O_3)$ on NOx concentrations along

431 with the normalized probability density (NPD) distribution of NOx concentrations at 5

432 m, 200 m, and 320 m in daytime during the field campaign. At different heights, $P(O_3)$

433 all rapidly increased with the rise in NOx until a critical NOx mixing ratio was reached,

434 after which $P(O_3)$ decreased slowly. The critical NOx mixing ratios decreased from

435 approximately 9.5 ppb at 5 m to 5.0 ppb at 320 m, primarily caused by the decreases in

436 both NOx concentrations and the OHRs of VOCs. As also shown in Fig. 8A, the

437 majority of the measured NOx mixing ratios fall into the transition zone of the $P(O_3)$-

438 NOx curves, suggesting that the photochemical ozone formation in Beijing belonged to

439 the transition regime below 320 m.

440   RIR values were also calculated using the box model results to further elucidate

441 the sensitivities of photochemical ozone formation to changes in multiple precursors at

442 different altitudes. As shown in Fig. 8B, positive RIR values were observed for both

443 NOx and various VOC groups at the five heights, further confirming that the

444 photochemical ozone formation belonged to the transition regime in the lower layer.

445 RIR values for NOx rapidly declined from 5 to 320 m, implying that the photochemical

446 ozone formation in higher altitudes was more prone to be controlled by the abundance

447 of VOCs. This is also manifested by the increasing RIR values for both AVOCs and

448 OVOCs from 5 m to 320 m. RIR values for BVOCs significantly decreased with height

449 due to their rapid removal by reactions with OH radicals when being vertically mixed.

450 These results are consistent with the results in section 3.3 that the less reactive AVOCs

451 and OVOCs are the dominant species in regulating the photochemical formation of

452 ozone in urban regions aloft.

453   According to the vertical distribution patterns of the photochemical ozone

454 formation regime, $P(O_3)$ decreases with increasing height alongside simultaneous

455   declines in concentrations of both NOx and VOCs. Fig. 8C presents the average diurnal

456   and vertical variations in $P(O_3)$ calculated by the box model during the campaign. The

457    $P(O_3)$ values were higher in daytime and correlated well with $j(NO_2)$. $P(O_3)$ decreased

458   from the ground to 320 m, where it still maintained a relatively high value of

459   approximately 10 ppb h^{-1} at noon. These results highlight that the photochemical

460   formation of ozone aloft also remained strong compared to those at ground level.

461   Consequently, the downward transport of ozone from high altitudes, driven by

462   turbulence mixing, can become significant sources of surface ozone during the day

463   *(Karl et al., 2023)*.

464   Due to the measurement height limitation, the vertical distributions of $P(O_3)$ in the

465   middle and upper parts of the PBL were not determined in this study. As reported by

466   the work in *(Benish et al., 2020)*, $P(O_3)$ typically exhibited weak and nearly linear

467   decline tendencies from 300 m to the top of the PBL during daytime. $P(O_3)$ at the PBL

468   top was approximately half of that at 300 m. Consequently, we can assume that $P(O_3)$

469   decreased linearly from 320 m to the top of the PBL. The integral of $P(O_3)$ at different

470   heights within the PBL can then be estimated using a similar method as described in

471   Eq. (5).

472   As shown in Fig. 8D, the total amount of ozone photochemically produced below

473   47 m constituted a mere 6% of the entire PBL. This fractional contribution increased to

474   approximately 35% at 320 m, further corroborating that the majority of the boundary-

475   layer ozone was produced in the middle and upper layers. Given the enhancement of

476   turbulence vertical mixing in daytime, ozone produced at high altitudes becomes a

477   significant source of surface ozone. This is substantiated by the widespread reports of

478   strong downward ozone fluxes in the bottom part of the PBL (tens of meters above

479   ground level) *(Fares et al., 2010; Liu et al., 2021; Karl et al., 2023)*. Consequently,

480   when devising ozone control strategies, particularly in urban regions with intricate

481   precursor emissions, careful considerations should be given to the vertical variations in

482   the formation regimes of ozone in the PBL.

4 Conclusions

The inadequate vertical distribution data of volatile organic compounds (VOCs) poses a significant barrier to fully comprehending the mechanisms underlying photochemical ozone formation and devising effective mitigation strategies. To address this concern, ~~In this study,~~ we made vertical gradient measurements ~~investigated the vertical variations, key drivers, and environmental impacts~~ of VOCs, NOx, and ozone ~~in the PBL~~ based on a 325 m tall tower ~~using tower-based online gradient measurements~~ in urban Beijing during the summer of 2021. This study offered more exhaustive and nuanced insights into the vertical variability of VOCs compared to previous studies. ~~The diurnal and vertical variations of various VOC species~~ Our findings underscored that the vertical variations of VOCs were strictly regulated by the diurnal evolution of the PBL and chemical processes. In daytime, reactive NMHCs ~~species were~~ were rapidly oxidized when they ~~were~~ were mixed upward along with the formation of OVOCs. As a result, concentrations of NMHCs decreased with height and many of OVOC species increased with height. OVOC species played more significant roles in regulating the photochemical ozone formation in urban regions aloft.

Model simulations unveiled that ~~The~~ the photochemical formation of ozone belongs to the transition regime in the lower ~~part of the~~ PBL and bec~~o~~ames more sensitive to changes in the concentrations of AVOCs and OVOCs with ~~increasing~~ height. With the further increase in height, the photochemical formation of ozone may change to the NOx control regime due to the total OHR of VOCs decreased much slower than NOx concentrations. $P(O_3)$ exhibited decreasing tendencies with height due to coupled declines in concentrations of NOx and VOCs. ~~but~~ $P(O_3)$ still remained ~~very~~ large in high altitudes, likely driven by ~~the~~ high OVOC concentrations ~~of OVOCs and OH radicals~~. This implies that the bulk of ozone formation occurs within the middle and upper strata of the PBL rather than proximate to the ground surface. Therefore, regional ozone control strategies necessitate meticulous consideration of vertical gradients in $P(O_3)$ and the varying regimes of photochemical ozone formation throughout the entire PBL ~~careful consideration should be given to the vertical~~

512 ~~variations in both P(O₃) and photochemical ozone formation regimes in the whole PBL~~
513 ~~when making regional ozone control strategies~~.

514   The vertical variations in concentrations and compositions of VOCs significantly
515 influence ~~the~~ ozone formation ~~of secondary pollutants~~. ~~Furthermore~~In addition, the
516 vertical changes in chemical reaction environments (e.g., temperature, humidity, and
517 solar radiation) and concentrations of other chemicals (e.g., particulate matters, NOx,
518 ozone) can also impact the degradation pathways of VOCs. These factors also affect
519 the formation pathways and production yields of other secondary air pollutants, such as
520 formic acid, isocyanic acid, and ~~secondary pollutants~~secondary organic aerosol. This is
521 particularly crucial for the highly reactive NMHCs in urban areas with complex
522 anthropogenic and biogenic emissions ~~and is expected to be thoroughly elucidated in~~
523 ~~future studies~~.

524   Limitations of our study include the confinement of measurements below 320
525 meters due to the tower's height, leaving the mid and upper daytime PBL's VOC
526 distributions and chemistries unexplored. Additionally, the absence of measurements
527 for some key chemical species like HONO, organic aerosol components, and reactive
528 halogen species might have implications for the accuracy of our box model results.
529 Future endeavors could integrate multiple observational techniques to capture a broader
530 vertical scope and a more comprehensive suite of species, thereby enhancing our
531 understanding of how vertical variations in VOC chemistry impact secondary pollution
532 formation.

Data availability

534   The observational data used in this study are available from corresponding authors
535 upon request.

Author contributions

537   BY, XBL, and YH designed the research. XBL, BY, YH, XS, JQ, XH, SW, YC,
538 QY, YS, YP, GT, JG, and MS contributed to the data collection and data analysis. XBL,

539 SY, and BY designed and performed the box model simulations. XBL and BY wrote
540 the paper with contributions from all coauthors. All the coauthors discussed the results
541 and reviewed the paper.

Competing interests

543 The authors declare that they have no conflict of interest.

Acknowledgments

545 The authors would like to thank the personnel who participated in data collection,
546 instrument maintenance, and logistic support during the field campaign.

Financial support

548 This work was financially supported by the National Key R&D Plan of China
549 (grant nos. 2023YFC3706103, 2023YFC3706201, 2023YFC3710900, and
550 2022YFC3700604) and the National Natural Science Foundation of China (grant nos.
551 42121004, 42275103, 42205094, 42230701, 42305095, and 42475107). This work was
552 also supported by the Guangdong Basic and Applied Basic Research Foundation (grant
553 no. 2024A1515011570) and Guangzhou Basic and Applied Basic Research Foundation
554 (grant no. 2024A04J3958).

References

556 An, J., Huang, Y., Huang, C., Wang, X., Yan, R., Wang, Q., Wang, H., Jing, S., Zhang,
557 Y., Liu, Y., Chen, Y., Xu, C., Qiao, L., Zhou, M., Zhu, S., Hu, Q., Lu, J., and Chen, C.:
558 Emission inventory of air pollutants and chemical speciation for specific anthropogenic
559 sources based on local measurements in the Yangtze River Delta region, China, Atmos.
560 Chem. Phys., 21, 2003-2025,https://doi.org/10.5194/acp-21-2003-2021 2021.
561 Atkinson, R., and Arey, J.: Atmospheric Degradation of Volatile Organic Compounds,
562 Chem Rev, 103, 4605-4638,https://doi.org/10.1021/cr0206420 2003.
563 Benish, S. E., He, H., Ren, X., Roberts, S. J., Salawitch, R. J., Li, Z., Wang, F., Wang,
564 Y., Zhang, F., Shao, M., Lu, S., and Dickerson, R. R.: Measurement report: Aircraft
565 observations of ozone, nitrogen oxides, and volatile organic compounds over Hebei
566 Province, China, Atmos. Chem. Phys., 20, 14523-14545,https://doi.org/10.5194/acp-
567 20-14523-2020 2020.

568 Brown, S. S., Dubé, W. P., Osthoff, H. D., Wolfe, D. E., Angevine, W. M., and
569 Ravishankara, A. R.: High resolution vertical distributions of NO_3 and N_2O_5 through
570 the nocturnal boundary layer, Atmos. Chem. Phys., 7, 139-149,10.5194/acp-7-139-
571 2007 2007.
572 Cooper, O. R., Schultz, M. G., Schroeder, S., Chang, K.-L., Gaudel, A., Benitez, G. C.,
573 Cuevas, E., Froehlich, M., Galbally, I. E., Molloy, S., Kubistin, D., Lu, X., McClure-
574 Begley, A., Nedelec, P., O'Brien, J., Oltmans, S. J., Petropavlovskikh, I., Ries, L., Senik,
575 I., Sjoeberg, K., Solberg, S., Spain, G. T., Spangl, W., Steinbacher, M., Tarasick, D.,
576 Thouret, V., and Xu, X.: Multi-decadal surface ozone trends at globally distributed
577 remote   locations,   Elementa-Science   of   the   Anthropocene,
578 8,https://doi.org/10.1525/elementa.420 2020.
579 Dieu Hien, V. T., Lin, C., Thanh, V. C., Kim Oanh, N. T., Thanh, B. X., Weng, C.-E.,
580 Yuan, C.-S., and Rene, E. R.: An overview of the development of vertical sampling
581 technologies for ambient volatile organic compounds (VOCs), J Environ Manage, 247,
582 401-412,https://doi.org/10.1016/j.jenvman.2019.06.090 2019.
583 Fares, S., McKay, M., Holzinger, R., and Goldstein, A. H.: Ozone fluxes in a Pinus
584 ponderosa ecosystem are dominated by non-stomatal processes: Evidence from long-
585 term   continuous   measurements,   Agr   Forest   Meteorol,   150,   420-
586 431,https://doi.org/10.1016/j.agrformet.2010.01.007 2010.
587 Fleming, Z. L., Doherty, R. M., von Schneidemesser, E., Malley, C. S., Cooper, O. R.,
588 Pinto, J. P., Colette, A., Xu, X., Simpson, D., Schultz, M. G., Lefohn, A. S., Hamad, S.,
589 Moolla, R., Solberg, S., and Feng, Z.: Tropospheric Ozone Assessment Report: Present-
590 day ozone distribution and trends relevant to human health, Elementa-Science of the
591 Anthropocene, 6,10.1525/elementa.273 2018.
592 Geng, C., Wang, J., Yin, B., Zhao, R., Li, P., Yang, W., Xiao, Z., Li, S., Li, K., and Bai,
593 Z.: Vertical distribution of volatile organic compounds conducted by tethered balloon
594 in the Beijing-Tianjin-Hebei region of China, Journal of Environmental Sciences, 95,
595 121-129,https://doi.org/10.1016/j.jes.2020.03.026 2020.
596 Geyer, A., and Stutz, J.: Vertical profiles of NO_3, N_2O_5, O_3, and NOx in the nocturnal
597 boundary layer: 2. Model studies on the altitude dependence of composition and
598 chemistry,   Journal   of   Geophysical   Research: Atmospheres,
599 109,https://doi.org/10.1029/2003jd004211 2004.
600 Gkatzelis, G. I., Coggon, M. M., McDonald, B. C., Peischl, J., Gilman, J. B., Aikin, K.
601 C., Robinson, M. A., Canonaco, F., Prevot, A. S. H., Trainer, M., and Warneke, C.:
602 Observations Confirm that Volatile Chemical Products Are a Major Source of
603 Petrochemical Emissions in U.S. Cities, Environ Sci Technol, 55, 4332-
604 4343,10.1021/acs.est.0c05471 2021.
605 Gómez, M. C., Durana, N., García, J. A., de Blas, M., Sáez de Cámara, E., García-Ruiz,
606 E., Gangoiti, G., Torre-Pascual, E., and Iza, J.: Long-term measurement of biogenic
607 volatile organic compounds in a rural background area: Contribution to ozone
608 formation,   Atmos   Environ,   224,
609 117315,https://doi.org/10.1016/j.atmosenv.2020.117315 2020.
610 Guo, H., Ling, Z. H., Cheng, H. R., Simpson, I. J., Lyu, X. P., Wang, X. M., Shao, M.,
611 Lu, H. X., Ayoko, G., Zhang, Y. L., Saunders, S. M., Lam, S. H. M., Wang, J. L., and

612   Blake, D. R.: Tropospheric volatile organic compounds in China, Sci Total Environ,
613   574, 1021-1043,https://doi.org/10.1016/j.scitotenv.2016.09.116 2017.

614   Guo, J.-X., Zeng, Y., Zhu, K., and Tan, X.: Vehicle mix evaluation in Beijing's
615   passenger-car sector: From air pollution control perspective, Sci Total Environ, 785,
616   147264,https://doi.org/10.1016/j.scitotenv.2021.147264 2021.

617   He, G., He, C., Wang, H., Lu, X., Pei, C., Qiu, X., Liu, C., Wang, Y., Liu, N., Zhang,
618   J., Lei, L., Liu, Y., Wang, H., Deng, T., Fan, Q., and Fan, S.: Nighttime ozone in the
619   lower boundary layer: insights from 3-year tower-based measurements in South China
620   and regional air quality modeling, Atmos. Chem. Phys., 23, 13107-13124,10.5194/acp-
621   23-13107-2023 2023.

622   He, X., Yuan, B., Wu, C., Wang, S., Wang, C., Huangfu, Y., Qi, J., Ma, N., Xu, W.,
623   Wang, M., Chen, W., Su, H., Cheng, Y., and Shao, M.: Volatile organic compounds in
624   wintertime North China Plain: Insights from measurements of proton transfer reaction
625   time-of-flight mass spectrometer (PTR-ToF-MS), J Environ Sci (China), 114, 98-
626   114,10.1016/j.jes.2021.08.010 2022.

627   Hofzumahaus, A., Rohrer, F., Lu, K., Bohn, B., Brauers, T., Chang, C.-C., Fuchs, H.,
628   Holland, F., Kita, K., Kondo, Y., Li, X., Lou, S., Shao, M., Zeng, L., Wahner, A., and
629   Zhang, Y.: Amplified Trace Gas Removal in the Troposphere, Science, 324, 1702-
630   1704,doi:10.1126/science.1164566 2009.

631   Karl, T., Lamprecht, C., Graus, M., Cede, A., Tiefengraber, M., Vila-Guerau de
632   Arellano, J., Gurarie, D., and Lenschow, D.: High urban NOx triggers a substantial
633   chemical downward flux of ozone, Science Advances, 9,
634   eadd2365,doi:10.1126/sciadv.add2365 2023.

635   Kaser, L., Patton, E. G., Pfister, G. G., Weinheimer, A. J., Montzka, D. D., Flocke, F.,
636   Thompson, A. M., Stauffer, R. M., and Halliday, H. S.: The effect of entrainment
637   through atmospheric boundary layer growth on observed and modeled surface ozone in
638   the Colorado Front Range, Journal of Geophysical Research: Atmospheres, 122, 6075-
639   6093,10.1002/2016jd026245 2017.

640   Kim, S., Seco, R., Gu, D., Sanchez, D., Jeong, D., Guenther, A. B., Lee, Y., Mak, J. E.,
641   Su, L., Kim, D. B., Lee, Y., Ahn, J.-Y., McGee, T., Sullivan, J., Long, R., Brune, W.
642   H., Thames, A., Wisthaler, A., Mueller, M., Mikoviny, T., Weinheimer, A., Yang, M.,
643   Woo, J.-H., Kim, S., and Park, H.: The role of a suburban forest in controlling vertical
644   trace gas and OH reactivity distributions - a case study for the Seoul metropolitan area,
645   Faraday Discuss, 226, 537-550,10.1039/d0fd00081g 2021.

646   Li, C., Liu, Y., Cheng, B., Zhang, Y., Liu, X., Qu, Y., An, J., Kong, L., Zhang, Y.,
647   Zhang, C., Tan, Q., and Feng, M.: A comprehensive investigation on volatile organic
648   compounds (VOCs) in 2018 in Beijing, China: Characteristics, sources and behaviours
649   in response to O3 formation, Sci Total Environ, 806,
650   150247,https://doi.org/10.1016/j.scitotenv.2021.150247 2022a.

651   Li, X.-B., Wang, D., Lu, Q.-C., Peng, Z.-R., Fu, Q., Hu, X.-M., Huo, J., Xiu, G., Li, B.,
652   Li, C., Wang, D.-S., and Wang, H.: Three-dimensional analysis of ozone and $PM_{2.5}$
653   distributions obtained by observations of tethered balloon and unmanned aerial vehicle
654   in Shanghai, China, Stoch Env Res Risk A, 32, 1189-
655   1203,https://doi.org/10.1007/s00477-018-1524-2 2018.

Li, X.-B., and Fan, G.: Interannual variations, sources, and health impacts of the springtime ozone in Shanghai, Environ Pollut, 306, 119458,https://doi.org/10.1016/j.envpol.2022.119458 2022.

Li, X.-B., Yuan, B., Parrish, D. D., Chen, D., Song, Y., Yang, S., Liu, Z., and Shao, M.: Long-term trend of ozone in southern China reveals future mitigation strategy for air pollution, Atmos Environ, 269, 118869,10.1016/j.atmosenv.2021.118869 2022b.

Li, X.-B., Yuan, B., Wang, S., Wang, C., Lan, J., Liu, Z., Song, Y., He, X., Huangfu, Y., Pei, C., Cheng, P., Yang, S., Qi, J., Wu, C., Huang, S., You, Y., Chang, M., Zheng, H., Yang, W., Wang, X., and Shao, M.: Variations and sources of volatile organic compounds (VOCs) in urban region: insights from measurements on a tall tower, Atmos. Chem. Phys., 22, 10567-10587,10.5194/acp-22-10567-2022 2022c.

Li, X.-B., Zhang, C., Liu, A., Yuan, B., Yang, H., Liu, C., Wang, S., Huangfu, Y., Qi, J., Liu, Z., He, X., Song, X., Chen, Y., Peng, Y., Zhang, X., Zheng, E., Yang, L., Yang, Q., Qin, G., Zhou, J., and Shao, M.: Assessment of long tubing in measuring atmospheric trace gases: applications on tall towers, Environmental Science: Atmospheres, 3, 506-520,10.1039/d2ea00110a 2023.

Li, X., Wang, W., Yang, S., Cheng, Y., Zeng, L., Yu, X., Lu, S., Liu, Y., Hu, M., Xie, S., Huang, X., Zhou, J., Shi, L., Xu, H., Lin, S., Liu, H., Feng, M., Song, D., Tan, Q., and Zhang, Y.: Ozone sensitivity regimes vary at different heights in the planetary boundary layer, Sci Total Environ, 944, 173712,https://doi.org/10.1016/j.scitotenv.2024.173712 2024.

Liu, X., Deming, B., Pagonis, D., Day, D. A., Palm, B. B., Talukdar, R., Roberts, J. M., Veres, P. R., Krechmer, J. E., Thornton, J. A., de Gouw, J. A., Ziemann, P. J., and Jimenez, J. L.: Effects of gas–wall interactions on measurements of semivolatile compounds and small polar molecules, Atmos. Meas. Tech., 12, 3137-3149,10.5194/amt-12-3137-2019 2019.

Liu, Y., Tang, G., Wang, Y., Cheng, M., Gao, J., and Wang, Y.: Spatiotemporal differences in tropospheric ozone sensitivity and the impact of "dual carbon" goal, Science Bulletin, 69, 422-425,https://doi.org/10.1016/j.scib.2023.12.026 2024a.

Liu, Y., Yin, S., Zhang, S., Ma, W., Zhang, X., Qiu, P., Li, C., Wang, G., Hou, D., Zhang, X., An, J., Sun, Y., Li, J., Zhang, Z., Chen, J., Tian, H., Liu, X., and Liu, L.: Drivers and impacts of decreasing concentrations of atmospheric volatile organic compounds (VOCs) in Beijing during 2016–2020, Sci Total Environ, 906, 167847,https://doi.org/10.1016/j.scitotenv.2023.167847 2024b.

Liu, Z., Pan, Y., Song, T., Hu, B., Wang, L., and Wang, Y.: Eddy covariance measurements of ozone flux above and below a southern subtropical forest canopy, Sci Total Environ, 791, 148338,https://doi.org/10.1016/j.scitotenv.2021.148338 2021.

Lu, K. D., Rohrer, F., Holland, F., Fuchs, H., Bohn, B., Brauers, T., Chang, C. C., Häseler, R., Hu, M., Kita, K., Kondo, Y., Li, X., Lou, S. R., Nehr, S., Shao, M., Zeng, L. M., Wahner, A., Zhang, Y. H., and Hofzumahaus, A.: Observation and modelling of OH and HO_2 concentrations in the Pearl River Delta 2006: a missing OH source in a VOC rich atmosphere, Atmos. Chem. Phys., 12, 1541-1569,10.5194/acp-12-1541-2012 2012.

699   Lu, Y., Pang, X., Lyu, Y., Li, J., Xing, B., Chen, J., Mao, Y., Shang, Q., and Wu, H.:
700   Characteristics and sources analysis of ambient volatile organic compounds in a typical
701   industrial park: Implications for ozone formation in 2022 Asian Games, Sci Total
702   Environ, 848, 157746,https://doi.org/10.1016/j.scitotenv.2022.157746 2022.
703   Ma, Z., Xu, H., Meng, W., Zhang, X., Xu, J., Liu, Q., and Wang, Y.: Vertical ozone
704   characteristics in urban boundary layer in Beijing, Environ Monit Assess, 185, 5449-
705   5460,10.1007/s10661-012-2958-5 2013.
706   Mo, Z., Shao, M., Wang, W., Liu, Y., Wang, M., and Lu, S.: Evaluation of biogenic
707   isoprene emissions and their contribution to ozone formation by ground-based
708   measurements in Beijing, China, Sci Total Environ, 627, 1485-
709   1494,https://doi.org/10.1016/j.scitotenv.2018.01.336 2018.
710   Mo, Z., Huang, S., Yuan, B., Pei, C., Song, Q., Qi, J., Wang, M., Wang, B., Wang, C.,
711   Li, M., Zhang, Q., and Shao, M.: Deriving emission fluxes of volatile organic
712   compounds from tower observation in the Pearl River Delta, China, Sci Total Environ,
713   741, 139763,https://doi.org/10.1016/j.scitotenv.2020.139763 2020.
714   Niu, H., Li, K., Chu, B., Su, W., and Li, J.: Heterogeneous Reactions between Toluene
715   and NO_2 on Mineral Particles under Simulated Atmospheric Conditions, Environ Sci
716   Technol, 51, 9596-9604,https://doi.org/10.1021/acs.est.7b00194 2017.
717   Ou, J., Zheng, J., Li, R., Huang, X., Zhong, Z., Zhong, L., and Lin, H.: Speciated OVOC
718   and VOC emission inventories and their implications for reactivity-based ozone control
719   strategy in the Pearl River Delta region, China, Sci Total Environ, 530-531, 393-
720   402,https://doi.org/10.1016/j.scitotenv.2015.05.062 2015.
721   Ou, J., Yuan, Z., Zheng, J., Huang, Z., Shao, M., Li, Z., Huang, X., Guo, H., and Louie,
722   P. K. K.: Ambient Ozone Control in a Photochemically Active Region: Short-Term
723   Despiking or Long-Term Attainment?, Environ Sci Technol, 50, 5720-
724   5728,https://doi.org/10.1021/acs.est.6b00345 2016.
725   Pagonis, D., Krechmer, J. E., de Gouw, J., Jimenez, J. L., and Ziemann, P. J.: Effects
726   of gas–wall partitioning in Teflon tubing and instrumentation on time-resolved
727   measurements of gas-phase organic compounds, Atmos. Meas. Tech., 10, 4687-
728   4696,10.5194/amt-10-4687-2017 2017.
729   Perdigones, B. C., Lee, S., Cohen, R. C., Park, J.-H., and Min, K.-E.: Two Decades of
730   Changes in Summertime Ozone Production in California's South Coast Air Basin,
731   Environ Sci Technol, 56, 10586-10595,10.1021/acs.est.2c01026 2022.
732   Qi, J., Mo, Z., Yuan, B., Huang, S., Huangfu, Y., Wang, Z., Li, X., Yang, S., Wang,
733   W., Zhao, Y., Wang, X., Wang, W., Liu, K., and Shao, M.: An observation approach in
734   evaluation of ozone production to precursor changes during the COVID-19 lockdown,
735   Atmos Environ, 262, 118618,https://doi.org/10.1016/j.atmosenv.2021.118618 2021.
736   Sangiorgi, G., Ferrero, L., Perrone, M. G., Bolzacchini, E., Duane, M., and Larsen, B.
737   R.: Vertical distribution of hydrocarbons in the low troposphere below and above the
738   mixing height: Tethered balloon measurements in Milan, Italy, Environ Pollut, 159,
739   3545-3552,https://doi.org/10.1016/j.envpol.2011.08.012 2011.
740   Shao, M., Wang, W., Yuan, B., Parrish, D. D., Li, X., Lu, K., Wu, L., Wang, X., Mo,
741   Z., Yang, S., Peng, Y., Kuang, Y., Chen, W., Hu, M., Zeng, L., Su, H., Cheng, Y.,
742   Zheng, J., and Zhang, Y.: Quantifying the role of PM2.5 dropping in variations of

ground-level ozone: Inter-comparison between Beijing and Los Angeles, Sci Total Environ, 147712,https://doi.org/10.1016/j.scitotenv.2021.147712 2021.

Song, X., Li, X.-B., Yuan, B., He, X., Chen, Y., Wang, S., Huangfu, Y., Peng, Y., Zhang, C., Liu, A., Yang, H., Liu, C., Li, J., and Shao, M.: Elucidating key factors in regulating budgets of ozone and its precursors in atmospheric boundary layer, npj Climate and Atmospheric Science, 7, 262,10.1038/s41612-024-00818-8 2024.

Souri, A. H., Nowlan, C. R., Wolfe, G. M., Lamsal, L. N., Chan Miller, C. E., Abad, G. G., Janz, S. J., Fried, A., Blake, D. R., Weinheimer, A. J., Diskin, G. S., Liu, X., and Chance, K.: Revisiting the effectiveness of HCHO/NO2 ratios for inferring ozone sensitivity to its precursors using high resolution airborne remote sensing observations in a high ozone episode during the KORUS-AQ campaign, Atmos Environ, 224, 117341,https://doi.org/10.1016/j.atmosenv.2020.117341 2020.

Sun, J., Wang, Y., Wu, F., Tang, G., Wang, L., Wang, Y., and Yang, Y.: Vertical characteristics of VOCs in the lower troposphere over the North China Plain during pollution periods, Environ Pollut, 236, 907-915,https://doi.org/10.1016/j.envpol.2017.10.051 2018.

Tang, G., Zhu, X., Xin, J., Hu, B., Song, T., Sun, Y., Zhang, J., Wang, L., Cheng, M., Chao, N., Kong, L., Li, X., and Wang, Y.: Modelling study of boundary-layer ozone over northern China - Part I: Ozone budget in summer, Atmos Res, 187, 128-137,https://doi.org/10.1016/j.atmosres.2016.10.017 2017.

Velasco, E., Marquez, C., Bueno, E., Bernabe, R. M., Sanchez, A., Fentanes, O., Wohrnschimmel, H., Cardenas, B., Kamilla, A., Wakamatsu, S., and Molina, L. T.: Vertical distribution of ozone and VOCs in the low boundary layer of Mexico City, Atmos. Chem. Phys., 8, 3061-3079,https://doi.org/10.5194/acp-8-3061-2008 2008.

Vo, T.-D.-H., Lin, C., Weng, C.-E., Yuan, C.-S., Lee, C.-W., Hung, C.-H., Bui, X.-T., Lo, K.-C., and Lin, J.-X.: Vertical stratification of volatile organic compounds and their photochemical product formation potential in an industrial urban area, J Environ Manage, 217, 327-336,https://doi.org/10.1016/j.jenvman.2018.03.101 2018.

Wang, C., Yuan, B., Wu, C., Wang, S., Qi, J., Wang, B., Wang, Z., Hu, W., Chen, W., Ye, C., Wang, W., Sun, Y., Wang, C., Huang, S., Song, W., Wang, X., Yang, S., Zhang, S., Xu, W., Ma, N., Zhang, Z., Jiang, B., Su, H., Cheng, Y., Wang, X., and Shao, M.: Measurements of higher alkanes using NO+ chemical ionization in PTR-ToF-MS: important contributions of higher alkanes to secondary organic aerosols in China, Atmos. Chem. Phys., 20, 14123-14138,https://doi.org/10.5194/acp-20-14123-2020 2020a.

Wang, H., Ma, X., Tan, Z., Wang, H., Chen, X., Chen, S., Gao, Y., Liu, Y., Liu, Y., Yang, X., Yuan, B., Zeng, L., Huang, C., Lu, K., and Zhang, Y.: Anthropogenic monoterpenes aggravating ozone pollution, Natl Sci Rev, 9, nwac103,10.1093/nsr/nwac103 2022a.

Wang, N., Lyu, X., Deng, X., Huang, X., Jiang, F., and Ding, A.: Aggravating O3 pollution due to NOx emission control in eastern China, Sci Total Environ, 677, 732-744,https://doi.org/10.1016/j.scitotenv.2019.04.388 2019.

785 Wang, N., Huang, X., Xu, J., Wang, T., Tan, Z.-m., and Ding, A.: Typhoon-boosted
786 biogenic emission aggravates cross-regional ozone pollution in China, Science
787 Advances, 8, eabl6166,doi:10.1126/sciadv.abl6166 2022b.
788 Wang, W., Qi, J., Zhou, J., Yuan, B., Peng, Y., Wang, S., Yang, S., Williams, J., Sinha,
789 V., and Shao, M.: The improved comparative reactivity method (ICRM): measurements
790 of OH reactivity under high-NOx conditions in ambient air, Atmos. Meas. Tech., 14,
791 2285-2298,10.5194/amt-14-2285-2021 2021a.
792 Wang, W., Yuan, B., Peng, Y., Su, H., Cheng, Y., Yang, S., Wu, C., Qi, J., Bao, F.,
793 Huangfu, Y., Wang, C., Ye, C., Wang, Z., Wang, B., Wang, X., Song, W., Hu, W.,
794 Cheng, P., Zhu, M., Zheng, J., and Shao, M.: Direct observations indicate
795 photodegradable oxygenated volatile organic compounds (OVOCs) as larger
796 contributors to radicals and ozone production in the atmosphere, Atmos. Chem. Phys.,
797 22, 4117-4128,10.5194/acp-22-4117-2022 2022c.
798 Wang, W., Li, X., Cheng, Y., Parrish, D. D., Ni, R., Tan, Z., Liu, Y., Lu, S., Wu, Y.,
799 Chen, S., Lu, K., Hu, M., Zeng, L., Shao, M., Huang, C., Tian, X., Leung, K. M., Chen,
800 L., Fan, M., Zhang, Q., Rohrer, F., Wahner, A., Pöschl, U., Su, H., and Zhang, Y.:
801 Ozone pollution mitigation strategy informed by long-term trends of atmospheric
802 oxidation capacity, Nature Geoscience, 17, 20-25,10.1038/s41561-023-01334-9 2024.
803 Wang, Y., Wang, Y., Tang, G., Yang, Y., Li, X., Yao, D., Wu, S., Kang, Y., Wang, M.,
804 and Wang, Y.: High gaseous carbonyl concentrations in the upper boundary layer in
805 Shijiazhuang, China, Sci Total Environ, 799,
806 149438,https://doi.org/10.1016/j.scitotenv.2021.149438 2021b.
807 Wang, Y. H., Gao, W. K., Wang, S., Song, T., Gong, Z. Y., Ji, D. S., Wang, L. L., Liu,
808 Z. R., Tang, G. Q., Huo, Y. F., Tian, S. L., Li, J. Y., Li, M. G., Yang, Y., Chu, B. W.,
809 Petaja, T., Kerminen, V. M., He, H., Hao, J. M., Kulmala, M., Wang, Y. S., and Zhang,
810 Y. H.: Contrasting trends of $PM_{2.5}$ and surface-ozone concentrations in China from
811 2013 to 2017, National Science Review, 7, 1331-
812 1339,https://doi.org/10.1093/nsr/nwaa032 2020b.
813 Wolfe, G. M., Marvin, M. R., Roberts, S. J., Travis, K. R., and Liao, J.: The Framework
814 for 0-D Atmospheric Modeling (F0AM) v3.1, Geoscientific Model Development, 9,
815 3309-3319,10.5194/gmd-9-3309-2016 2016.
816 Wu, C., Wang, C., Wang, S., Wang, W., Yuan, B., Qi, J., Wang, B., Wang, H., Wang,
817 C., Song, W., Wang, X., Hu, W., Lou, S., Ye, C., Peng, Y., Wang, Z., Huangfu, Y., Xie,
818 Y., Zhu, M., Zheng, J., Wang, X., Jiang, B., Zhang, Z., and Shao, M.: Measurement
819 report: Important contributions of oxygenated compounds to emissions and chemistry
820 of volatile organic compounds in urban air, Atmos. Chem. Phys., 20, 14769-
821 14785,https://doi.org/10.5194/acp-20-14769-2020 2020.
822 Yang, Q., Li, X. B., Yuan, B., Zhang, X., Huangfu, Y., Yang, L., He, X., Qi, J., and
823 Shao, M.: Measurement report: Enhanced photochemical formation of formic and
824 isocyanic acids in urban regions aloft – insights from tower-based online gradient
825 measurements, Atmos. Chem. Phys., 24, 6865-6882,10.5194/acp-24-6865-2024 2024a.
826 Yang, S., Yuan, B., Peng, Y., Huang, S., Chen, W., Hu, W., Pei, C., Zhou, J., Parrish,
827 D. D., Wang, W., He, X., Cheng, C., Li, X. B., Yang, X., Song, Y., Wang, H., Qi, J.,
828 Wang, B., Wang, C., Wang, C., Wang, Z., Li, T., Zheng, E., Wang, S., Wu, C., Cai, M.,

829 Ye, C., Song, W., Cheng, P., Chen, D., Wang, X., Zhang, Z., Wang, X., Zheng, J., and
830 Shao, M.: The formation and mitigation of nitrate pollution: comparison between urban
831 and suburban environments, Atmos. Chem. Phys., 22, 4539-4556,10.5194/acp-22-
832 4539-2022 2022.
833 Yang, X., Wang, H., Lu, K., Ma, X., Tan, Z., Long, B., Chen, X., Li, C., Zhai, T., Li,
834 Y., Qu, K., Xia, Y., Zhang, Y., Li, X., Chen, S., Dong, H., Zeng, L., and Zhang, Y.:
835 Reactive aldehyde chemistry explains the missing source of hydroxyl radicals, Nature
836 Communications, 15, 1648,10.1038/s41467-024-45885-w 2024b.
837 Ye, C., Yuan, B., Lin, Y., Wang, Z., Hu, W., Li, T., Chen, W., Wu, C., Wang, C., Huang,
838 S., Qi, J., Wang, B., Wang, C., Song, W., Wang, X., Zheng, E., Krechmer, J. E., Ye, P.,
839 Zhang, Z., Wang, X., Worsnop, D. R., and Shao, M.: Chemical characterization of
840 oxygenated organic compounds in the gas phase and particle phase using iodide CIMS
841 with FIGAERO in urban air, Atmos. Chem. Phys., 21, 8455-
842 8478,https://doi.org/10.5194/acp-21-8455-2021 2021.
843 Yeo, M. J., and Kim, Y. P.: Long-term trends of surface ozone in Korea, Journal of
844 Cleaner Production, 294, 125352,https://doi.org/10.1016/j.jclepro.2020.125352 2021.
845 Yuan, B., Koss, A. R., Warneke, C., Coggon, M., Sekimoto, K., and de Gouw, J. A.:
846 Proton-Transfer-Reaction Mass Spectrometry: Applications in Atmospheric Sciences,
847 Chem Rev, 117, 13187-13229,https://doi.org/10.1021/acs.chemrev.7b00325 2017.
848 Zhang, K., Xiu, G., Zhou, L., Bian, Q., Duan, Y., Fei, D., Wang, D., and Fu, Q.: Vertical
849 distribution of volatile organic compounds within the lower troposphere in late spring
850 of Shanghai, Atmos Environ, 186, 150-
851 157,https://doi.org/10.1016/j.atmosenv.2018.03.044 2018.
852 Zhang, Y., Xue, L., Mu, J., Chen, T., Li, H., Gao, J., and Wang, W.: Developing the
853 Maximum Incremental Reactivity for Volatile Organic Compounds in Major Cities of
854 Central-Eastern China, Journal of Geophysical Research: Atmospheres, 127,
855 e2022JD037296,https://doi.org/10.1029/2022JD037296 2022.
856 Zhao, M., Zhang, Y., Pei, C., Chen, T., Mu, J., Liu, Y., Wang, Y., Wang, W., and Xue,
857 L.: Worsening ozone air pollution with reduced NOx and VOCs in the Pearl River Delta
858 region in autumn 2019: Implications for national control policy in China, J Environ
859 Manage, 324, 116327,https://doi.org/10.1016/j.jenvman.2022.116327 2022.

860
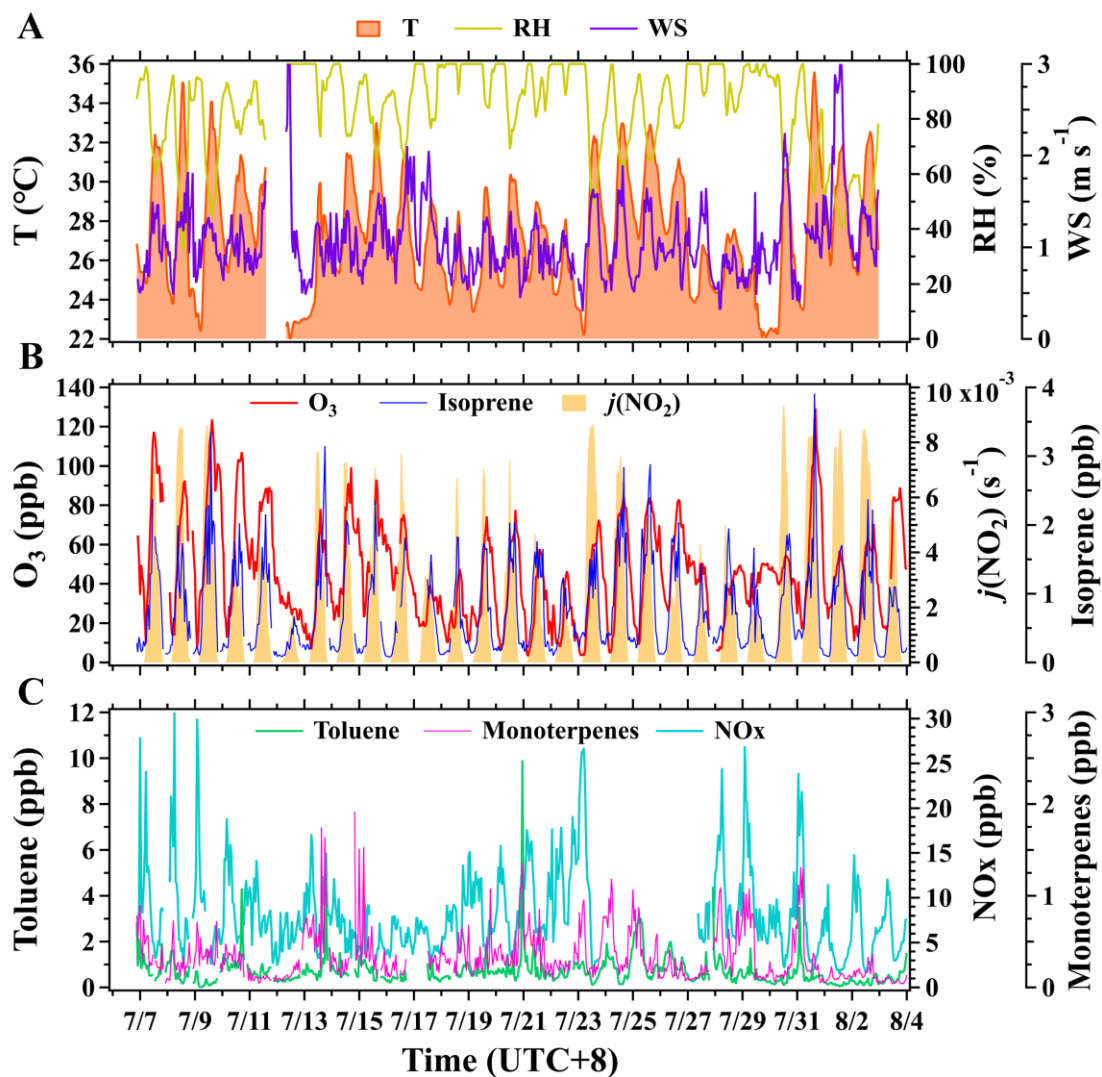
Figure 1. Time series of hourly mean air temperature (T), relative humidity (RH), wind

speed (WS), and mixing ratios of surface ozone, NOx, and VOC species along with

$j(NO_2)$ at the BMT site during the campaign. Meteorological parameters were measured

at 8 m above ground level and mixing ratios of ozone and its selected precursors were

measured at 5 m above ground level.

866
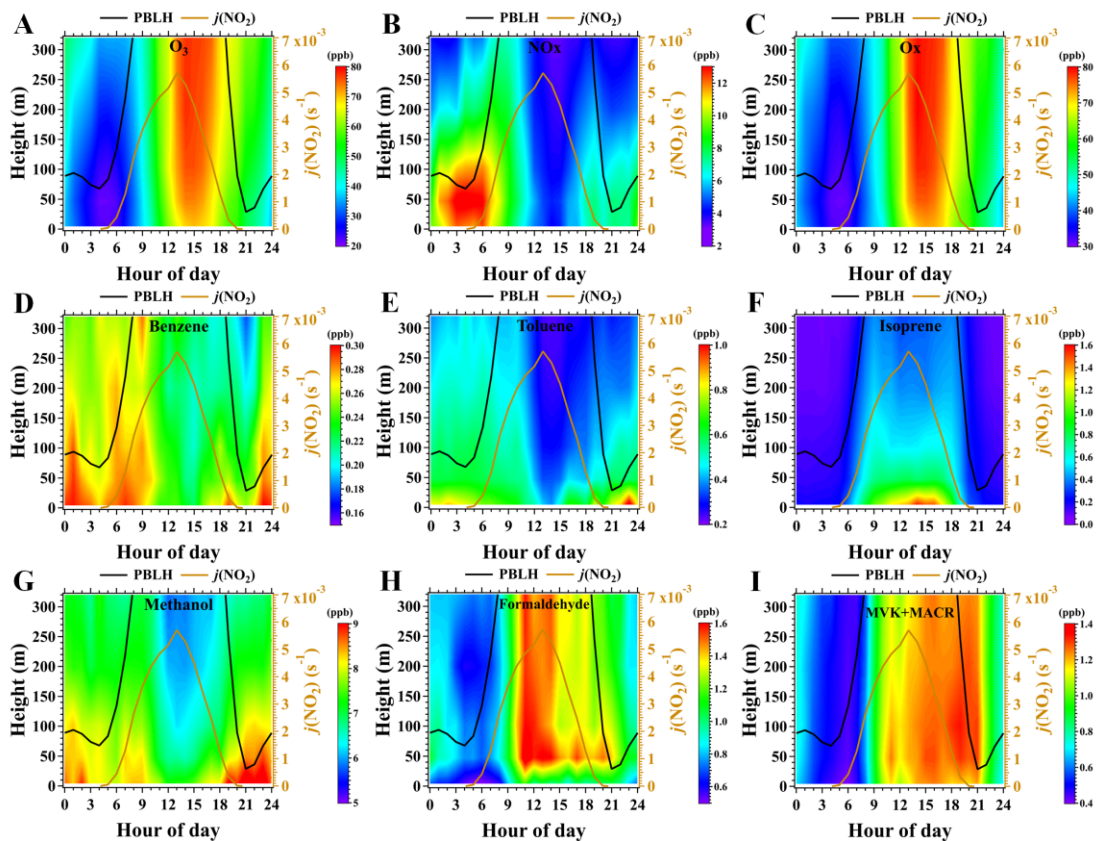
Figure 2. Average diurnal and vertical variations in mixing ratios of ozone, NOx, Ox
(O₃+NO₂), and six selected VOC species along with the average diurnal profiles of
PBLH and j(NO₂) during the campaign. The figures were obtained by linearly
interpolating the data at the five inlet heights on both altitude and temporal scales.

871
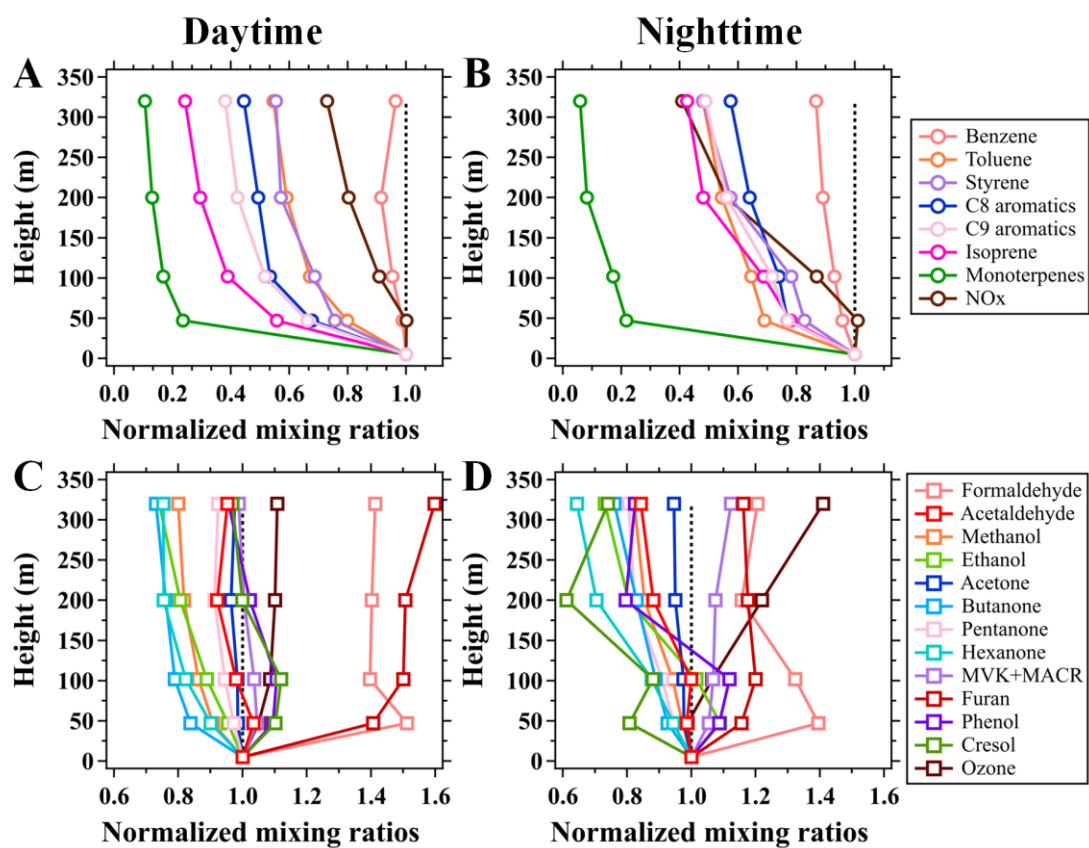
Figure 3. Average vertical profiles of (A-B) NMHCs and NOx, (C-D) OVOCs and O₃

during the daytime (11:00-16:00 LT) and nighttime (23:00-04:00 LT) of the campaign.

The mixing ratios of the chemical species measured above 5 m are normalized to those

at 5 m.

876
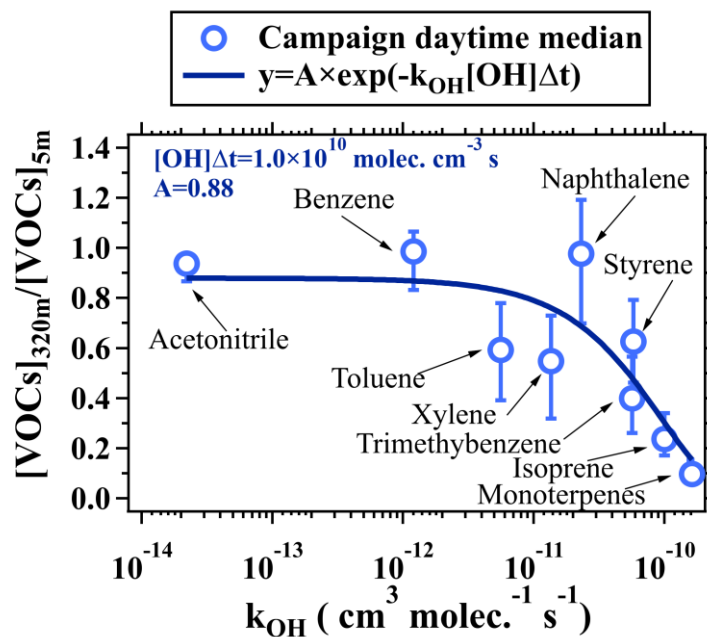
Figure 4. The change in ratios of NMHC concentrations (including acetonitrile) between 320 m and 5 m as a function of k_{OH}. The vertically-resolved measurements of VOCs made on the BMT in daytime during the campaign were used for analysis. Hollow markers represent median values and error bars indicate the range between 25th and 75th percentiles.

882
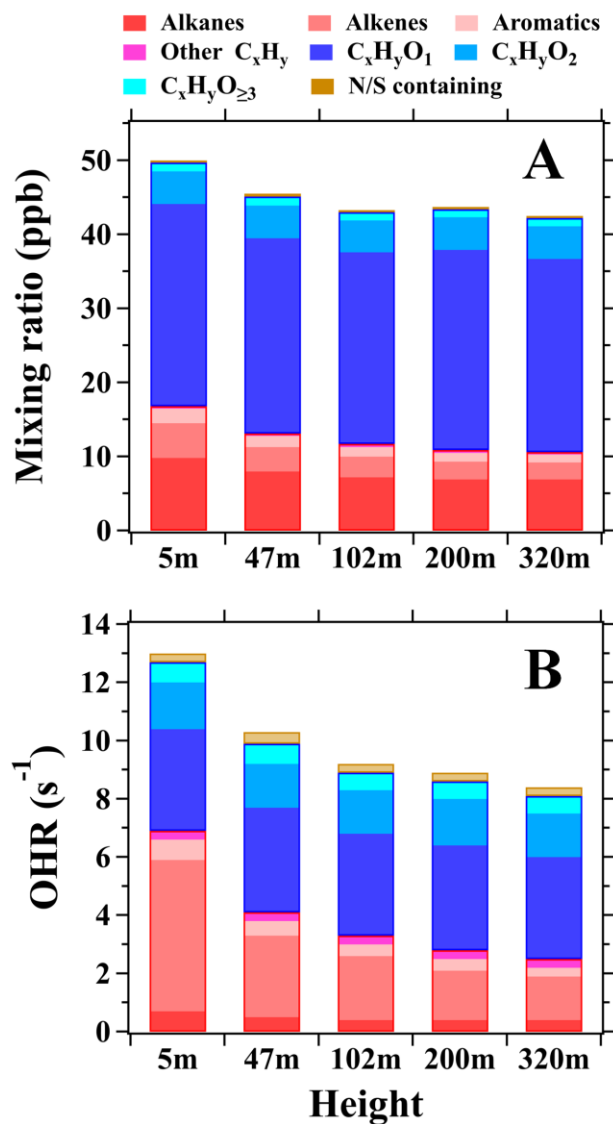
Figure 5. (A) Mean mixing ratios and (B) OHRs of different VOC categories at the five

inlet heights in daytime during the campaign.

885
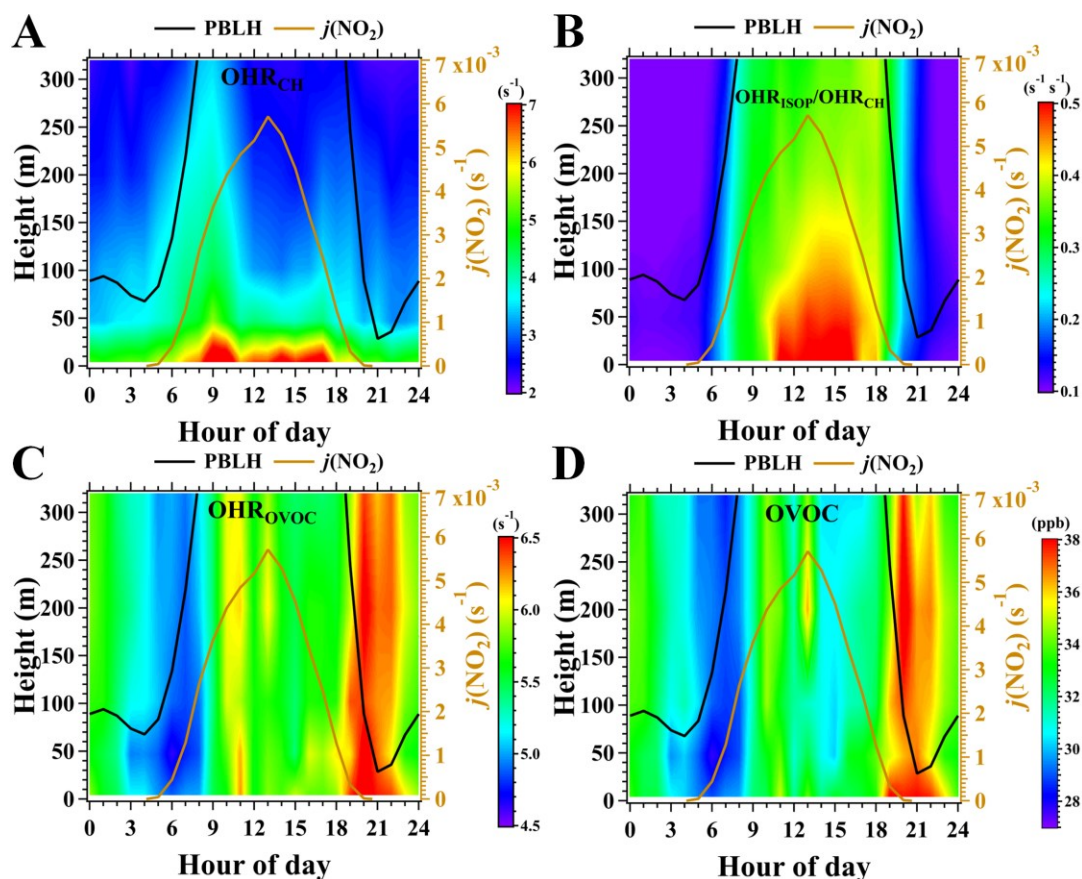
Figure 6. (A-B) Average diurnal and vertical variations in OHRs of C_xH_y and the OHR ratios of isoprene to C_xH_y (OHR$_{ISOP}$/OHR$_{CH}$) during the campaign. (C-D) Average diurnal and vertical variations in mixing ratios and OHRs of OVOC. ISOP refers to isoprene. The figures were obtained by linearly interpolating the data at the five measurement heights on both altitude and temporal scales.

891
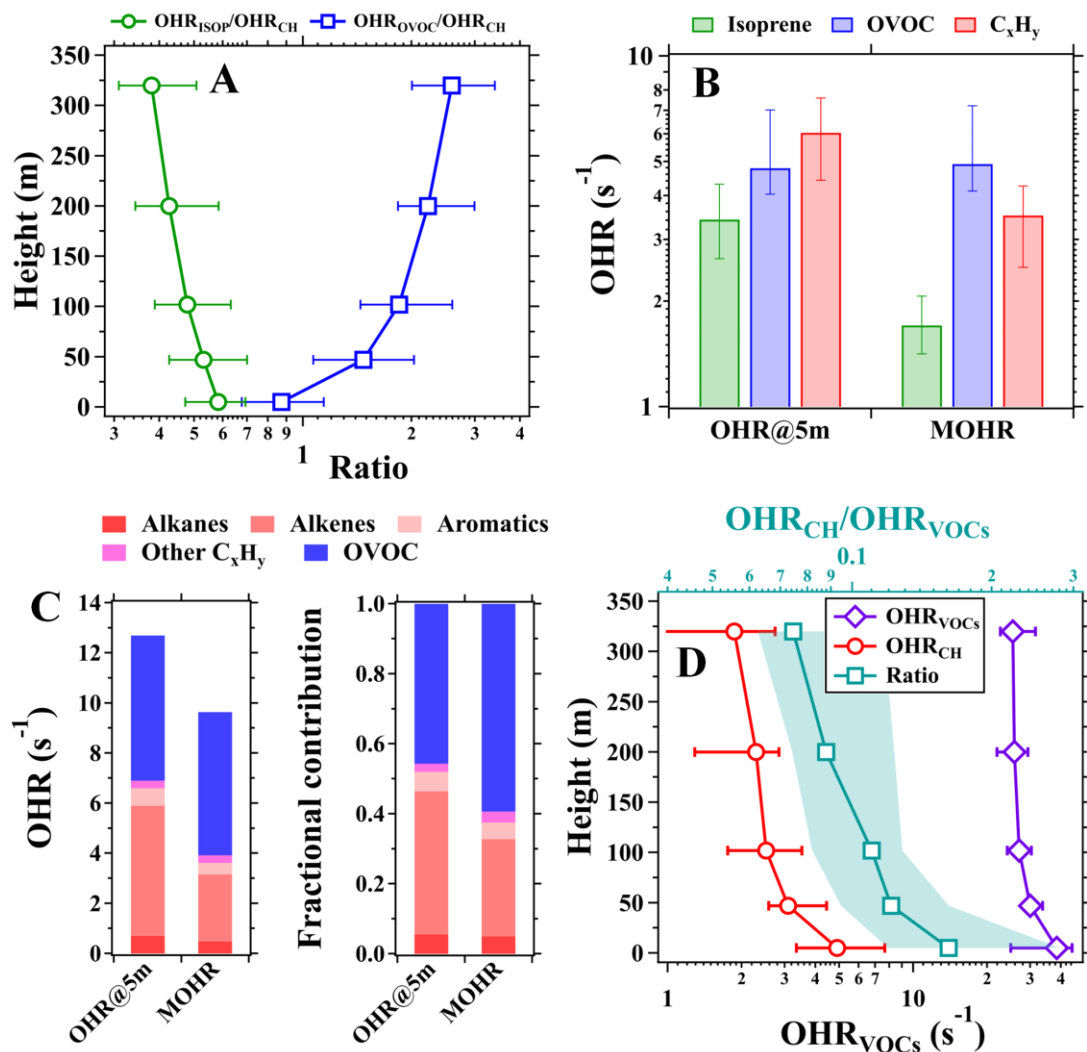
Figure 7. (A) Average vertical profiles of OHR ratios of isoprene to C_xH_y (OHR$_{ISOP}$/OHR$_{CH}$) and OVOC to NMHC (OHR$_{OVOC}$/OHR$_{CH}$). (B) Median values of the OHR at 5 m and the mean OHR (MOHR) between 5 m and 320 m for isoprene, OVOC, and C_xH_y. (C) Mean contributions of different VOC categories to the MOHR below 320 m and the OHR at 5 m. (D) Vertical profiles of the measured OHR$_{VOCs}$ and the calculated OHR$_{CH}$ (bottom axis) and the OHR$_{CH}$/OHR$_{VOCs}$ ratios (top axis) during July 28-31, 2021. The data used for analysis in panels A-D was within the time window from 11:00 to 16:00 LT during the campaign. Markers in panels A and D represent median values. Shaded areas and error bars in panels A, B, and D indicate the range between 25th and 75th percentiles.

902
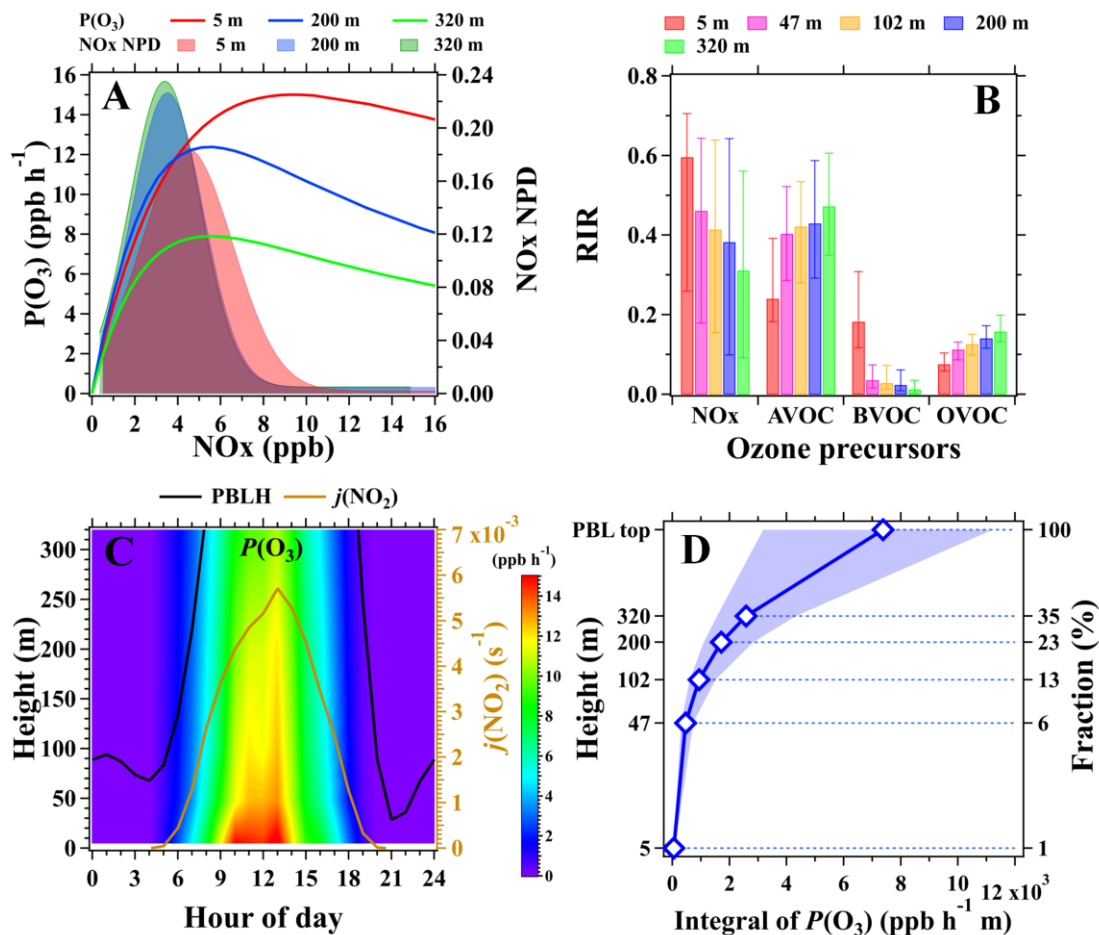
Figure 8. (A) Left axis: average dependence of P(O₃) on NOx concentrations in daytime during the campaign; Right axis: normalized probability density (NPD) of NOx mixing ratios in daytime at the three inlet heights. (B) Median RIR values of photochemical ozone formation to changes in NOx, AVOC (NMHCs excluding BVOC), BVOC (isoprene), and OVOC (nine OVOC species in Table S1) at the five inlet heights; Error bars indicate the range between 25th and 75th percentiles. (C) Average diurnal and vertical variations in P(O₃) during the campaign; The figure was obtained by linearly interpolating the data at the five measurement heights on both altitude and temporal scales. (D) The vertical profile of the integral of P(O₃) in daytime during the campaign; Markers indicate median values and Shaded areas indicate the range between 25th and 75th percentiles.